Quantum Emission from Defects in Single-Crystalline Hexagonal Boron Nitride

Toan Trong Tran,[1] Cameron Zachreson,[1] Amanuel Michael Berhane,[1] Kerem Bray,[1] Russell Guy Sandstrom,[1] Lu Hua Li,[2] Takashi Taniguchi,[3] Kenji Watanabe,[3] Igor Aharonovich,[1,*] and Milos Toth[1,†]

[1]*School of Mathematical and Physical Sciences, University of Technology Sydney, Ultimo, New South Wales 2007, Australia*

[2]*Institute of Frontier Materials, Deakin University, Geelong Waurn Ponds Campus, Victoria 3216, Australia*

[3]*National Institute for Materials Science, Namiki 1-1, Tsukuba, Ibaraki 305-0044, Japan*

(Received 31 July 2015; revised manuscript received 22 October 2015; published 10 March 2016)

Bulk hexagonal boron nitride (hBN) is a highly nonlinear natural hyperbolic material that attracts major attention in modern nanophotonics applications. However, studies of its optical properties in the visible part of the spectrum and quantum emitters hosted by bulk hBN have not been reported to date. In this work, we study the emission properties of hBN crystals in the red spectral range using sub-band-gap optical excitation. Quantum emission from defects is observed at room temperature and characterized in detail. Our results advance the use of hBN in quantum nanophotonics technologies and enhance our fundamental understanding of its optical properties.

DOI: 10.1103/PhysRevApplied.5.034005

I. INTRODUCTION

Recent studies have been focused on various wide-band-gap materials with superior chemical and thermal stability needed for optoelectronics and applications [1–5]. Bulk hexagonal boron nitride (hBN) is one of these materials and offers excellent thermal conductivity and bright luminescence in the deep ultraviolet (UV) region associated with band-edge transitions [6–11], which is highly advantageous for light-emitting devices. Despite numerous studies of these emissions by x-ray, electron energy loss, and luminescence spectroscopy techniques, exact models of the emissions remain under debate. This is in part due to the complicated growth techniques (often high pressure and temperature) that can give rise to significant numbers of dislocations, stacking faults, and impurity atoms, including oxygen and carbon. Furthermore, hBN is a naturally hyperbolic material. Its extreme optical anisotropy gives rise to potential interesting applications based on subwavelength confinement and strong light-matter interactions [12–14]. However, to fully exploit the potential of hBN for quantum nanophotonics applications, true single-photon emitters in this material must be identified.

Here, we report a comprehensive study of single-photon emitters in the visible and near-infrared regions hosted by bulk hBN crystals. Our results promote the use of hBN as an interesting candidate for emerging applications in quantum technologies and nanophotonics.

*Corresponding author.
Igor.Aharonovich@uts.edu.au
†Corresponding author.
Milos.Toth@uts.edu.au

II. EXPERIMENT

The hBN single crystals used in this work are produced by the high-temperature and high-pressure process [15]. The hBN crystals are annealed for 30 min at 850 °C under 0.5 Torr of argon in a conventional tube furnace. The samples are heated at a ramp rate of 2 °C/ sec from room temperature. Upon completion, the samples are cooled to room temperature overnight. The annealing process is used to increase the number of luminescent defect centers. Optical images are obtained using a Zeiss optical microscope. Raman spectroscopy is conducted using a Renishaw in Via Raman™ microscope. The confocal maps and single-photon spectroscopy are performed at room temperature using a continuous-wave (cw) 532-nm laser (Gem 532™, Laser Quantum Ltd.). The laser is directed through a Glan-Taylor polarizer (Thorlabs Inc.) and a half wave plate and focused onto the sample using a high-numerical-aperture (NA = 0.9, Nikon) objective lens. Scanning is performed using an X-Y piezo scanning mirror (FSM-300TM, Newport Corp.) or an X-Y-Z nanocube system (PI Instruments). The collected light is filtered using a 532-nm dichroic mirror (532-nm laser BrightLine™, Semrock Inc.) and an additional long-pass filter (SemrockTM). The signal is then coupled into a graded index fiber, where the fiber aperture serves as a confocal pinhole. A fiber splitter is used to direct the light into a spectrometer (Acton SpectraPro™, Princeton Instrument Inc.) or into two avalanche photodiodes (Excelitas Technologies™) used for single-photon counting. Correlation measurements are done using a time-correlated single-photon-counting module (PicoHarp300™, PicoQuant™). Lifetime measurements are performed using a 675-nm pulsed laser excitation source (PiL067X™, Advanced Laser Diode Systems™ GmbH) with a 45-ps pulse width.

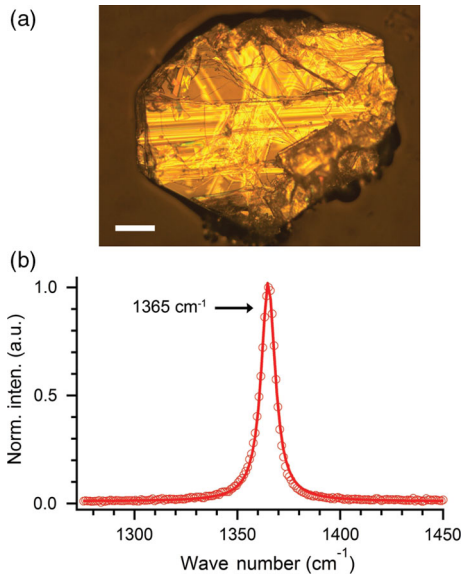

FIG. 1. (a) Optical microscope image of bulk hBN. The scale bar indicates 100 μm. (b) Raman scattering spectrum obtained with a 633-nm He-Ne laser showing a peak at 1365 cm^{-1} with a FWHM of 8.2 cm^{-1}.

III. RESULTS AND DISCUSSION

We start by surveying the sample using conventional optical microscopy and Raman spectroscopy, as shown in Fig. 1. The bulk crystal shows a number of visible stacking disorder lines [Fig. 1(a)]. Raman spectra of the sample exhibit the characteristic E_{2g} in-plane vibrational mode of bulk hexagonal boron nitride at 1365 cm^{-1}, with a full width at half maximum (FWHM) of 8.2 cm^{-1} [Fig. 1(b)], indicating that the sample is a high-quality crystal [16]. Additional characterization is performed using near-edge x-ray absorption fine structure (NEXAFS) and cathodoluminescence spectroscopy [17]. The results are provided in Supplemental Material, along with corresponding data from a second sample that contained a lower concentration of defects (as per NEXAFS and optical microscopy data) [17]. We note that the single-photon emitters characterized below (Figs. 2–4) are not found in this second sample.

Most prior luminescence studies of bulk hBN were performed using above-band-gap excitation (as in Fig. S2), whereby the emission spectra are typically dominated by UV or near-UV luminescence [17]. On the contrary, in this paper, we adopt the techniques used for other wide-band-gap materials, such as SiC and diamond, in order to access deep, defect-related levels preferentially and avoid transitions that entail the conduction and valence bands. Figure 2(a) shows a typical confocal photoluminescence (PL) map of the hBN crystal obtained using a 532-nm excitation laser and a shallow confocal depth of a few hundred nanometers, revealing an isolated emission (circled in red) along with other ensemble emissions. A background spectrum (dotted gray trace) obtained from a region adjacent to the emitter is shown in Fig. 2(b), revealing two Raman lines at 575 and 583 nm [18]. A PL spectrum taken from this particular defect [solid red trace in Fig. 2(b)] reveals two sharp peaks at 618 and 629 nm. Both peaks are potentially the zero-phonon lines (ZPLs) of a color center and are relatively close to the emission line in our previous report [19]. Correlation spectroscopy using a Hanbury-Brown–Twiss interferometer is therefore used to prove that the two peaks correspond to an isolated defect that emits single photons. Figure 2(c) displays the second-order autocorrelation measurement $g^2(\tau)$, showing that at zero delay time $g^2(0) \sim 0.35$ [Fig. 2(c), where the red dots are experimental data while the solid line is a fit obtained using a three-level model]. The $g^2(0)$ value of less than 0.5 proves unambiguously that the emitter is a single-photon source [20–22] (we note that the data are not corrected for the background which comprises approximately 30% of the total light intensity). On average, we find two such isolated emitters in each 60×60 μm^2 area of the sample.

The emission associated with the defect characterized in Fig. 2 bleaches after several minutes of excitation at

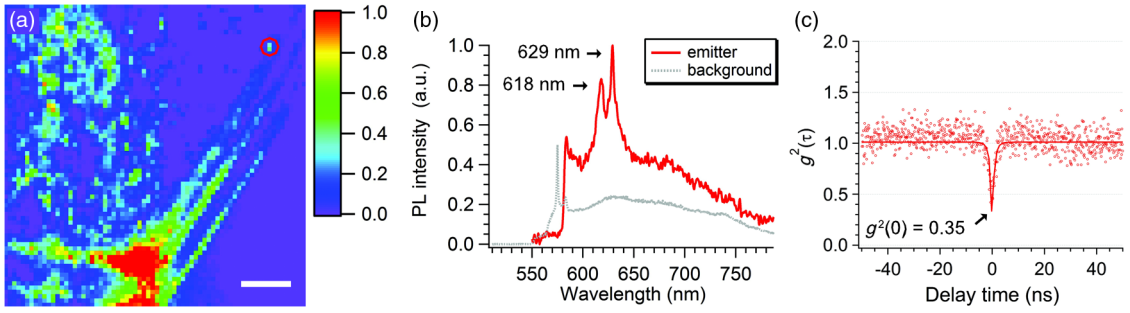

FIG. 2. Optical characterization performed with a 532-nm cw laser and a 568-nm long-pass filter in the collection pathway. (a) A typical confocal map of bulk hBN showing a number of isolated emission centers and ensembles of these centers. The scale bar indicates 10 μm. (b) A room-temperature photoluminescence spectrum of the isolated emission circled in the PL confocal map. The solid red and dotted gray traces represent the emitter and background spectra, respectively. The emitter spectrum reveals a pair of peaks at 618 and 629 nm that are potentially the zero-phonon lines of the defect transition. (c) An antibunching curve recorded from the defect center in (b) showing a dip of approximately 0.35, proving the single-photon emission nature of the defect. The bin size in (c) is 128 ps.

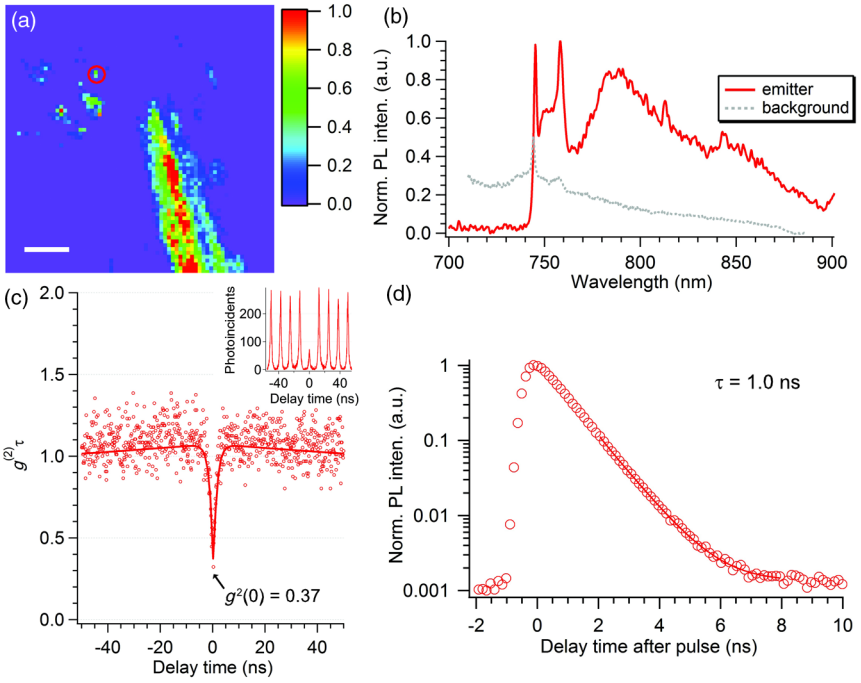

FIG. 3. (a) A typical confocal map showing isolated emission centers and ensembles of emitters. The scale bar indicates 10 μm. (b) A room-temperature PL spectrum of the isolated emission that is circled in the PL confocal map, revealing a broad emission band at approximately 770–900 nm. The solid red and dotted gray traces represent the emitter and background spectra, respectively. (c) An antibunching curve recorded by continuous-wave excitation of the defect center in (b) showing a dip of approximately 0.37, proving the quantum nature of the defect. The inset shows a similar antibunching curve obtained by pulsed excitation. (d) Time-resolved fluorescence measurement of the defect center in (b) revealing a very short radiative lifetime of approximately 1.0 ns. All measurements are done using a 675-nm cw laser at room temperature, with a 855 $\pm$ 110 nm band-pass filter. Pulsed $g^2(\tau)$ and lifetime measurements (d) are conducted using a 675-nm laser with a pulse width of 45 ps, a power of 200 μW, and repetition rate of 80 MHz. The bin size in (b) and (d) is 128 ps.

532 nm. To gain additional insights into the occurrence of emitters in hBN, we employ a longer excitation wavelength of 675 nm. A typical confocal map is shown in Fig. 3(a) and contains several isolated emission spots. Similar to the previous case, we find an average of two isolated emitters in each 60 × 60 μm^2 area of the sample. A PL spectrum (solid red trace) taken from one of these spots (circled in red) shows a broad emission band in the range of approximately 770–900 nm [Fig. 3(b)]. The dotted gray trace is the background luminescence [18]. We note that in Fig. 3(b) the line at approximately 745 nm is most likely background, as it appears in the gray curve as well, while the line at approximately 760 nm is a potential ZPL. A second-order autocorrelation function, $g^2(\tau)$, is shown in Fig. 3(c) (the red dots are experimental data, while the solid line is a fit obtained using a three-level model). A dip of approximately 0.37 at zero delay time confirms the single-photon-emission nature of the center. As our antibunching curve is obtained without background correction, the deviation from zero originates primarily from background emissions from the crystal. The inset in Fig. 3(c) demonstrates triggered single-photon emission using pulsed excitation, which is important for many practical nanophotonics applications.

Measurements of fluorescence intensity from the same defect as a function of excitation power show that the fluorescence saturates at a count rate slightly greater than 200 000 counts per second, comparable with other single-photon emitters in bulk materials [23]. Time-resolved fluorescence measurements yield a lifetime of approximately 1.0 ns [Fig. 3(d)]. This value is comparable to most conventional single emitters in bulk materials [23,24]. Polarization measurements are conducted using a combination of a linear half wave plate and/or a linear polarized filter (Supplemental Material [17], Fig. S3). The results show that the emission is fully linearly polarized.

The electron-phonon coupling characteristics of the two emitters are estimated using the Huang-Rhys (RH) factor. By fitting the PL spectra with multiple Lorentzian peaks, we calculated the RH factor to be 0.93 and 1.93 for the color centers shown in Figs. 2 and 3, respectively (in the case of the former, the analysis is done using the combined intensity of the two ZPLs and the total intensity of the broad phonon sideband emission, which is assumed to consist of two overlapping sidebands corresponding to the ZPLs). These values are in good agreement with prior literature [9].

To characterize the photodynamics of the defect shown in Fig. 3 further, time-correlated measurements are performed on the emitter. The detected photons are time-tagged over a long time scale, and the results are shown in Fig. 4(a). Three exponential components yield the best fit for the autocorrelation curve. This indicates that there are several additional metastable states associated with the electronic structure of this defect beside its principle radiative transition (i.e., between the ground state and the excited state). An illustration of such an excited electronic structure is shown in the inset in Fig. 4(a), with the lifetimes of the three additional metastable states 480 ns, 5 μs, and 31 ms, respectively. The transition rates to these states are relatively low, which explains why the defect can be detected on a single-photon level with reasonable brightness.

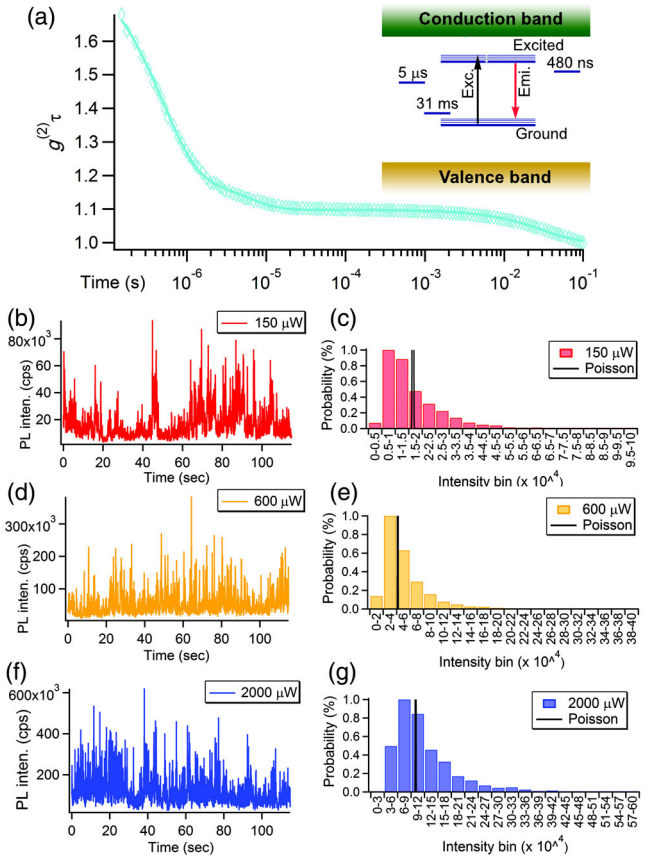

FIG. 4. (a) Long time-scale second-order autocorrelation function (recorded up to 0.1 s) reveals at least three possible metastable states of the defect center characterized in Fig. 3. The inset illustrates the possible excited electronic configuration of the defect center, including the existence of three metastable states. Temporal fluorescence intensity fluctuations at (b) 150, (d) 600, and (f) 2000 μW and the corresponding histograms at (c) 150, (e) 600, and (g) 2000 μW. The black traces in (c), (e), and (g) are corresponding simulated Poisson distributions, shown for comparison. The time-bin size in (b), (d), and (f) is 50 ms.

To elucidate the complex dynamics further, we characterize the blinking behavior of the defect at an elevated excitation power. Plots of fluorescence intensity are recorded as a function of time at excitation powers of 150 [Fig. 4(b)], 600 [Fig. 4(d)], and 2000 μW [Fig. 4(f)]. Blinking is clearly observed at all the investigated excitation powers. However, no bleaching of the defect is observed. This behavior is consistent with the autocorrelation function recorded in Fig. 4(a) and confirms the power dependence of the transition to the metastable states. Histograms of the fluorescence intensity [Figs. 4(c), 4(e), and 4(g)] reveal asymmetric distributions, rather than Poisson distributions expected from a nonblinking emitter, similar to that observed in ZnO nanoparticles [25]. Such behavior, often referred to as "photon bursts," is characteristic of an intermittent bright state. The severe spectral diffusion, seen clearly in an off-on histogram shown in Fig. S4 [17], is likely associated with the close proximity of the emitter to the surface or to extended defects. Given the wide band gap of hBN, it is expected that additional defects with other ZPL positions will be found, as in the case of shallow emitters in diamond [26].

We highlight differences between the current work and a recent report of quantum emitters in hBN [19]. First, the host materials are different, namely, the bulk, three-dimensional (3D) hBN crystal shown in Fig. 1(a), compared to two-dimensional (2D) hBN studied in Ref. [19]. Second, the emitters characterized in Figs. 2–4 exhibit different photophysical properties and temporal dynamics. Specifically, the emitter reported in Ref. [19] has characteristic PL spectra and photostability and photodynamics characteristics in monolayer hBN and in few-layer 2D hBN, all of which are different from those of the two emitters in bulk hBN reported here.

In addition, 2D materials have strong confinement in the direction perpendicular to their basal plane and are affected minimally by adjacent layers via van der Waals forces [27,28]. This may result in stronger dipole moments within the 2D monolayers. On the other hand, strain fields should be weaker in the 3D lattice, and emitters in bulk crystals are not expected to be affected as much by the environment. The unusual anisotropic dielectric environment in the 3D hBN lattice is predicted to provide extraordinary nonlinear optical properties such as subdiffraction focusing and guiding of emitted light that is of crucial importance for next-generation optoelectronic applications [12,29].

Finally, we note that it is important to identify and study emitters in both bulk and nanoscale materials, as they are used for entirely different applications. For instance, the bulk hBN studied here could be exploited in monolithic on-chip integrated photonic circuits [30], and it has hyperbolic properties [12,29] that do not exist in monolayer hBN.

IV. SUMMARY

In summary, room-temperature single-photon emission from bulk hBN is observed in the visible and the near-infrared spectral ranges. The longer wavelength center does not bleach and has a short lifetime of approximately 1 ns. The defect centers offer a class of a single-photon source to be realized based on bulk hBN. Our results enhance the present understanding of fundamental quantum phenomena in hBN and open the door to studies of light-matter interactions with quantum emitters in a hyperbolic medium.

ACKNOWLEDGMENTS

This research was partly undertaken on the soft x-ray beam line at the Australian Synchrotron, Victoria, Australia. The work was supported in part by the Australian Research Council (Project No. DP140102721) and FEI Company. I. A. is supported by an Australian Research Council Discovery Early Career Research Award

(Project No. DE130100592). Partial funding for this research was provided by the Air Force Office of Scientific Research, United States Air Force.

[1] I. Aharonovich and E. Neu, Diamond nanophotonics, Adv. Opt. Mater. **2**, 911 (2014).
[2] Y. Taniyasu, M. Kasu, and T. Makimoto, An aluminium nitride light-emitting diode with a wavelength of 210 nanometres, Nature (London) **441**, 325 (2006).
[3] C. Liu, Z. Hu, Q. Wu, X. Wang, Y. Chen, H. Sang, J. Zhu, S. Deng, and N. Xu, Vapor–solid growth and characterization of aluminum nitride nanocones, J. Am. Chem. Soc. **127**, 1318 (2005).
[4] Y. Lin and J. W. Connell, Advances in 2D boron nitride nanostructures: Nanosheets, nanoribbons, nanomeshes, and hybrids with graphene, Nanoscale **4**, 6908 (2012).
[5] K. Watanabe, T. Taniguchi, T. Niiyama, K. Miya, and M. Taniguchi, Far-ultraviolet plane-emission handheld device based on hexagonal boron nitride, Nat. Photonics **3**, 591 (2009).
[6] K. Watanabe, T. Taniguchi, and H. Kanda, Direct-bandgap properties and evidence for ultraviolet lasing of hexagonal boron nitride single crystal, Nat. Mater. **3**, 404 (2004).
[7] R. Bourrellier, M. Amato, L. H. Galvão Tizei, C. Giorgetti, A. Gloter, M. I. Heggie, K. March, O. Stéphan, L. Reining, M. Kociak, and A. Zobelli, Nanometric resolved luminescence in h-BN flakes: Excitons and stacking order, ACS Photonics **1**, 857 (2014).
[8] P. Jaffrennou, J. Barjon, J. S. Lauret, B. Attal-Trétout, F. Ducastelle, and A. Loiseau, Origin of the excitonic recombinations in hexagonal boron nitride by spatially resolved cathodoluminescence spectroscopy, J. Appl. Phys. **102**, 116102 (2007).
[9] L. Museur, E. Feldbach, and A. Kanaev, Defect-related photoluminescence of hexagonal boron nitride, Phys. Rev. B **78**, 155204 (2008).
[10] A. Pierret, J. Loayza, B. Berini, A. Betz, B. Plaçais, F. Ducastelle, J. Barjon, and A. Loiseau, Excitonic recombinations in h–BN: From bulk to exfoliated layers, Phys. Rev. B **89**, 035414 (2014).
[11] S. Meuret, L. H. G. Tizei, T. Cazimajou, R. Bourrellier, H. C. Chang, F. Treussart, and M. Kociak, Photon Bunching in Cathodoluminescence, Phys. Rev. Lett. **114**, 197401 (2015).
[12] J. D. Caldwell, A. V. Kretinin, Y. Chen, V. Giannini, M. M. Fogler, Y. Francescato, C. T. Ellis, J. G. Tischler, C. R. Woods, A. J. Giles, M. Hong, K. Watanabe, T. Taniguchi, S. A. Maier, and K. S. Novoselov, Sub-diffractional volume-confined polaritons in the natural hyperbolic material hexagonal boron nitride, Nat. Commun. **5**, 5221 (2014).
[13] S. Dai, Q. Ma, T. Andersen, A. S. McLeod, Z. Fei, M. K. Liu, M. Wagner, K. Watanabe, T. Taniguchi, M. Thiemens, F. Keilmann, P. Jarillo-Herrero, M. M. Fogler, and D. N. Basov, Subdiffractional focusing and guiding of polaritonic rays in a natural hyperbolic material, Nat. Commun. **6**, 6963 (2015).
[14] J. D. Caldwell, L. Lindsay, V. Giannini, I. Vurgaftman, T. L. Reinecke, S. A. Maier, and O. J. Glembocki, Low-loss, infrared and terahertz nanophotonics using surface phonon polaritons, Nanophotonics **4**, 44 (2015).
[15] T. Taniguchi and K. Watanabe, Synthesis of high-purity boron nitride single crystals under high pressure by using Ba–BN solvent, J. Cryst. Growth **303**, 525 (2007).
[16] Y. Kubota, K. Watanabe, O. Tsuda, and T. Taniguchi, Deep ultraviolet light-emitting hexagonal boron nitride synthesized at atmospheric pressure, Science **317**, 932 (2007).
[17] See Supplemental Material at http://link.aps.org/supplemental/10.1103/PhysRevApplied.5.034005 for additional characterization data obtained using near-edge x-ray absorption fine structure spectroscopy, Raman spectroscopy, cathodoluminescence spectroscopy, photoluminescence polarization, and a histogram of fluorescene on and off times from an emitter in bulk hBN.
[18] S. Reich, A. C. Ferrari, R. Arenal, A. Loiseau, I. Bello, and J. Robertson, Resonant Raman scattering in cubic and hexagonal boron nitride, Phys. Rev. B **71**, 205201 (2005).
[19] T. T. Tran, K. Bray, M. J. Ford, M. Toth, and I. Aharonovich, Quantum emission from hexagonal boron nitride monolayers, Nat. Nanotechnol. **11**, 37 (2016).
[20] C. Kurtsiefer, S. Mayer, P. Zarda, and H. Weinfurter, Stable Solid-State Source of Single Photons, Phys. Rev. Lett. **85**, 290 (2000).
[21] P. Michler *et al.*, A quantum dot single-photon turnstile device, Science **290**, 2282 (2000).
[22] B. Lounis and M. Orrit, Single-photon sources, Rep. Prog. Phys. **68**, 1129 (2005).
[23] S. Castelletto, B. C. Johnson, V. Ivády, N. Stavrias, T. Umeda, A. Gali, and T. Ohshima, A silicon carbide room-temperature single-photon source, Nat. Mater. **13**, 151 (2014).
[24] N. Elke, S. David, R.-M. Janine, G. Stefan, F. Martin, S. Matthias, and B. Christoph, Single photon emission from silicon-vacancy colour centres in chemical vapour deposition nano-diamonds on iridium, New J. Phys. **13**, 025012 (2011).
[25] O. Neitzke, A. Morfa, J. Wolters, A. W. Schell, G. Kewes, and O. Benson, Investigation of line width narrowing and spectral jumps of single stable defect centers in ZnO at cryogenic temperature, Nano Lett. **15**, 3024 (2015).
[26] D. Gatto Monticone, P. Traina, E. Moreva, J. Forneris, P. Olivero, I. P. Degiovanni, F. Taccetti, L. Giuntini, G. Brida, G. Amato, and M. Genovese, Native NIR-emitting single colour centres in CVD diamond, New J. Phys. **16**, 053005 (2014).
[27] F. Xia, H. Wang, D. Xiao, M. Dubey, and A. Ramasubramaniam, Two-dimensional material nanophotonics, Nat. Photonics **8**, 899 (2014).
[28] Q. H. Wang, K. Kalantar-Zadeh, A. Kis, J. N. Coleman, and M. S. Strano, Electronics and optoelectronics of two-dimensional transition metal dichalcogenides, Nat. Nanotechnol. **7**, 699 (2012).
[29] S. Dai, Z. Fei, Q. Ma, A. S. Rodin, M. Wagner, A. S. McLeod, M. K. Liu, W. Gannett, W. Regan, K. Watanabe, T. Taniguchi, M. Thiemens, G. Dominguez, A. H. C. Neto, A. Zettl, F. Keilmann, P. Jarillo-Herrero, M. M. Fogler, and D. N. Basov, Tunable phonon polaritons in atomically thin van der Waals crystals of boron nitride, Science **343**, 1125 (2014).
[30] P. Rath, S. Ummethala, C. Nebel, and W. H. P. Pernice, Diamond as a material for monolithically integrated optical and optomechanical devices, Phys. Status Solidi A **212**, 2385 (2015).